

(a)

DLAHDSEEL⁴⁷FQDLSQLQEAWLA⁵⁷EAEQVPDDEQ
EELFQDLSQ
SQLQEAWLA
EAWLAEAQV

9aa TAD Match

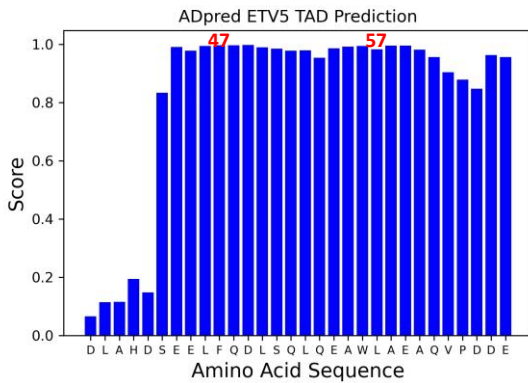
75%
75%
83%

(b)

APPTDVSLGDELHLDGEDVAMAHADALDD⁴³⁹FD⁴⁴²L⁴⁴⁴DMLGDGDS
DVAMAHADA
ADALDDFDL
DDFDLDMLG

75%
92%
100%

(c)



(d)

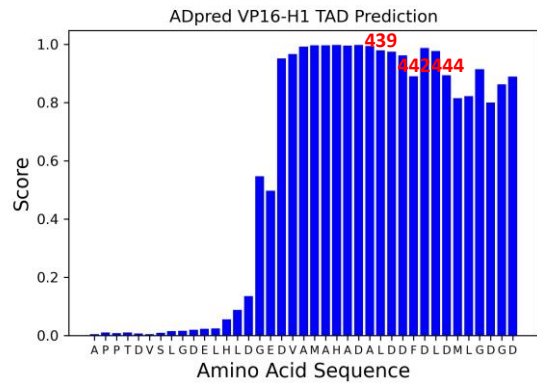


Figure S1. Matches within ETV5³⁸⁻⁶⁸ and VP16-H1⁴¹³⁻⁴⁵² TADs to activation domain consensus motifs. (a) Matches of ETV5³⁸⁻⁶⁸ to the '9aa TAD' consensus. Residues F⁴⁷ and W⁵⁷ are labelled with red numbers. The percentages of the motifs that are matching the 'low-stringency' consensus are shown on the right hand side in blue. (b) Same as in (a) but for VP16-H1⁴¹³⁻⁴⁵². Residues L⁴³⁹, F⁴⁴² and L⁴⁴⁴ are labelled with red numbers. (c) Matches of ETV5³⁸⁻⁶⁸ to a TAD consensus motif derived from yeast TADs. The highest score, 1.0, represents a perfect match. (d) Same as in (c) but for VP16-H1⁴¹³⁻⁴⁵². Predictions based on the 9aa TAD prediction tool on <https://www.med.muni.cz/9aaTAD/> (for panels [a] and [b]) and <https://adpred.fredhutch.org/> (panels [c] and [d]).

Secondary Structure Elements	ETV5 ³⁸⁻⁶⁸	ETV5 ³⁸⁻⁶⁸	VP16-H1 ⁴¹³⁻⁴⁵¹	VP16-H1 ⁴¹³⁻⁴⁵¹
β -Sheet (para)	0.22%	β-Sheet: 2.97%	0.75%	β-Sheet: 7.33%
β -Sheet (anti)	2.75%		6.58%	
3_{10} Helix	3.33%	α-Helix: 44.15%	5.65%	α-Helix: 45.89%
α -Helix	40.78%		40.08%	
π -Helix	0.04%		0.16%	
Turn	9.76%	Turn/Bend: 18.41%	19.59%	Turn/Bend: 32.42%
Bend	8.65%		12.83%	

Table S1. Detailed breakdown of secondary structure elements formed within ETV5³⁸⁻⁶⁸ and VP16-H1⁴¹³⁻⁴⁵² TADs after MCMC simulation. Both ETV5³⁸⁻⁶⁸ and VP16-H1⁴¹³⁻⁴⁵² TADs contain overall a similar proportion of α -helices that are formed transiently in absence of binding to a coactivator target, but VP16-H1⁴¹³⁻⁴⁵² contains a higher proportion of disorder-generating turns and bends.

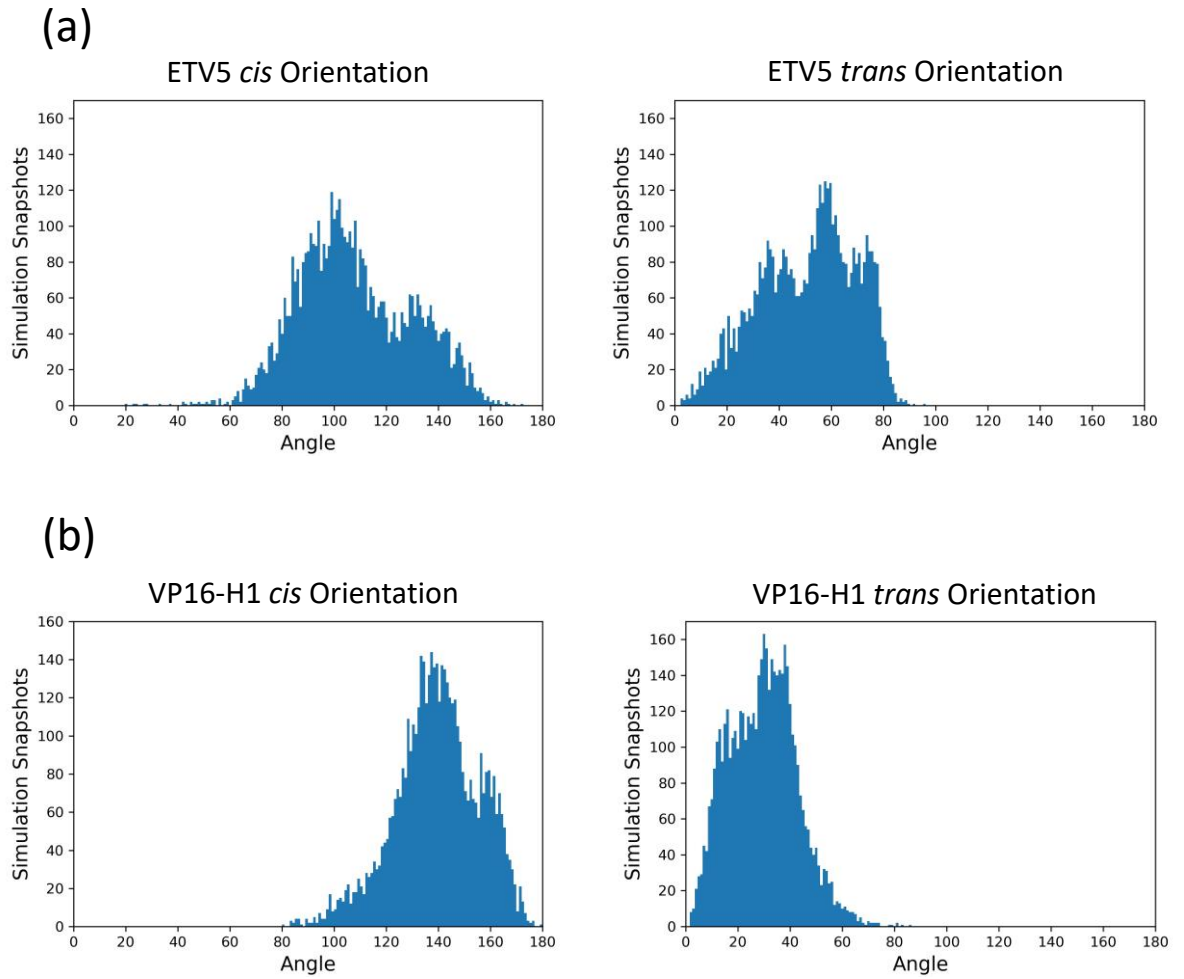
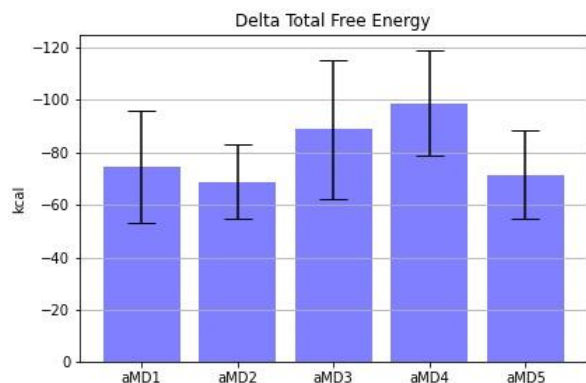
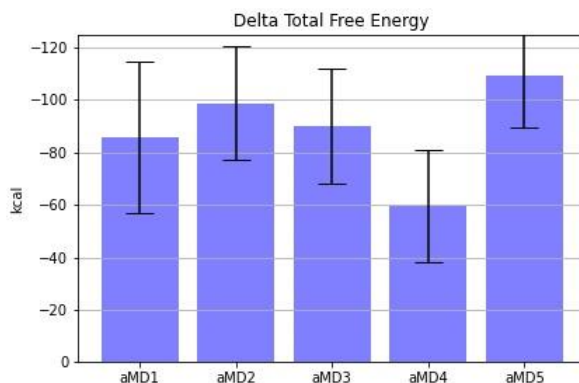


Figure S2. Distribution of angles between MED25 and TADs. (a) Distributions of angles between the α -helical portion of ETV5³⁸⁻⁶⁸ and the direction of the β 3 strand of MED25 in *cis*- and *trans*-orientations (left and right panel, respectively). (b) Same as in (a) but for VP16-H1⁴¹³⁻⁴⁵².

(a)**(b)****(c)**

	Average	Standard Deviation		Average	Standard Deviation		
aMD1	<i>cis</i>	-74.4	21.5	aMD1	<i>trans</i>	-85.8	28.9
aMD2	<i>cis</i>	-68.9	14.3	aMD2	<i>trans</i>	-98.8	21.8
aMD3	<i>cis</i>	-88.8	26.5	aMD3	<i>trans</i>	-89.0	21.9
aMD4	<i>cis</i>	-98.7	20.1	aMD4	<i>trans</i>	-59.6	21.3
aMD5	<i>cis</i>	-71.4	16.8	aMD5	<i>trans</i>	-109.5	19.9

Figure S3. MM-GBSA results of the total $\Delta G_{\text{Binding}}$ energy contributions of ETV5³⁸⁻⁶⁸ binding in (a) the *cis*-orientation, or (b) the *trans*-orientation. $\Delta G_{\text{Binding}}$ combines van der Waals and electrostatic interactions. (c) Table showing the values as numerical results. The data is averaged from five independent aMD simulations/panel (labelled on the x-axis) and the error bars show the standard deviation.

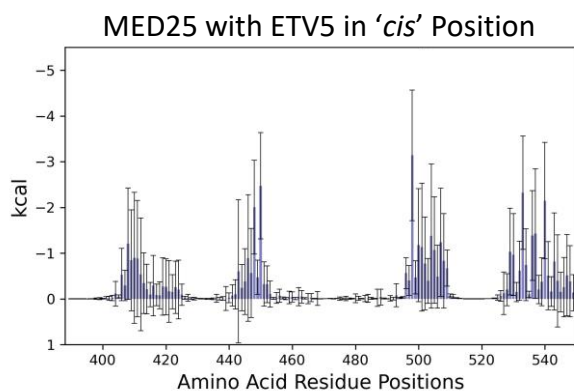
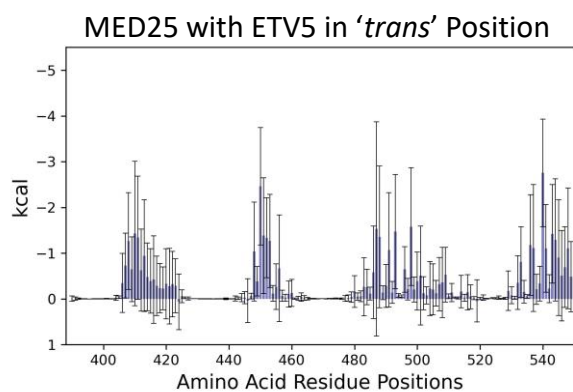
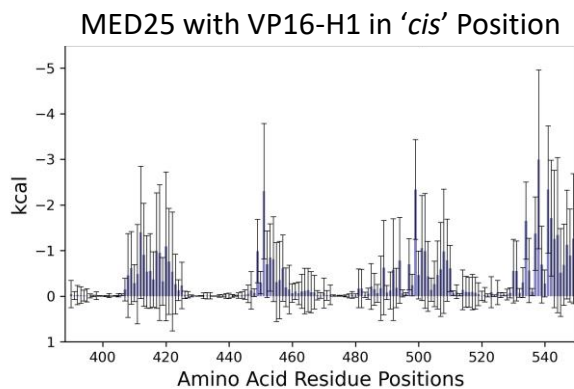
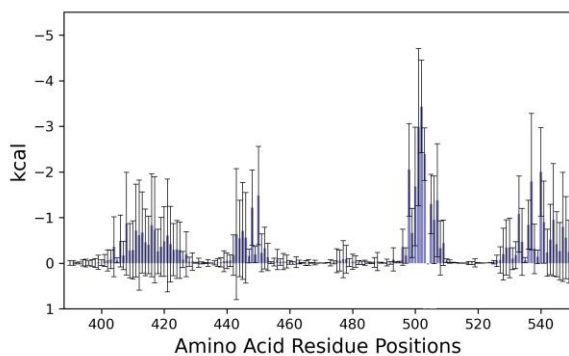
(a)**(b)****(c)****(d)**

Figure S4. MM-GBSA results of the van der Waals energy contributions of MED25 residues. Each data set shows the average value for each residue from five aMD simulations and the standard deviation as error bars. **(a)** Residue-specific energies during binding of ETV5³⁸⁻⁶⁸ in the *cis*-orientation. **(b)** Residue-specific energies during binding of ETV5³⁸⁻⁶⁸ in the *trans*-orientation. **(c)** Same as in (a) but for VP16-H1⁴¹³⁻⁴⁵². **(d)** Same as in (b) but for VP16-H1⁴¹³⁻⁴⁵².